JACS
JOURNAL OF THE AMERICAN CHEMICAL SOCIETY
Communication
pubs.acs.org/JACS

Selective Deposition of Ru Nanoparticles on $TiSi_2$ Nanonet and Its Utilization for Li_2O_2 Formation and Decomposition

Jin Xie,[†,§] Xiahui Yao,[†,§] Ian P. Madden,[†] De-En Jiang,[‡] Lien-Yang Chou,[†] Chia-Kuang Tsung,[†] and Dunwei Wang*[,†]

[†]Department of Chemistry, Merkert Chemistry Center, Boston College, 2609 Beacon Street, Chestnut Hill, Massachusetts 02467, United States

[‡]Chemical Sciences Division, Oak Ridge National Laboratory, Oak Ridge, Tennessee 37831, United States

Supporting Information

ABSTRACT: The Li−O_2 battery promises high capacity to meet the need for electrochemical energy storage applications. Successful development of the technology hinges on the availability of stable cathodes. The reactivity exhibited by a carbon support compromises the cyclability of Li−O_2 operation. A noncarbon cathode support has therefore become a necessity. Using a $TiSi_2$ nanonet as a high surface area, conductive support, we obtained a new noncarbon cathode material that corrects the deficiency. To enable oxygen reduction and evolution, Ru nanoparticles were deposited by atomic layer deposition onto $TiSi_2$ nanonets. A surprising site-selective growth whereupon Ru nanoparticles only deposit onto the b planes of $TiSi_2$ was observed. DFT calculations show that the selectivity is a result of different interface energetics. The resulting heteronanostructure proves to be a highly effective cathode material. It enables Li−O_2 test cells that can be recharged more than 100 cycles with average round-trip efficiencies >70%.

Modern technological developments have made electrical energy storage an indispensable need in society. Existing battery technologies, Li-ion batteries being the state-of-the-art, do not meet our demands in terms of energy capacity and power density.[1] Significant research is required to bridge the gap. The capacity of batteries can be readily increased if we move away from intercalation chemistry that powers Li-ion batteries and turn to conversion reactions. The Li−O_2 battery, enabled by the conversion between O_2 and Li_2O_2, is expected to offer one of the highest capacities. For this reason, it has received rapidly growing attention.[2−4] Before the potential of the Li−O_2 technology can be fully realized, however, a number of important issues must be addressed. At the center of these issues are the poor cyclability and low discharge/charge efficiency. It is recently recognized that these issues are intimately connected to the electrode design, the choice of electrolyte, and their interactions.[5,6] In particular, the widely used carbon support has been shown unstable under Li−O_2 operation conditions.[5,7] Because the purported reversible Li_2O_2 formation and decomposition primarily take place on the surface of the carbon cathode, the instability of carbon poses a significant challenge. The problem can in principle be solved by replacing carbon with other cathode materials.[8−10] Here we present the $TiSi_2$ nanonet as a new, noncarbon cathode support that permits Li−O_2 operations for over 100 cycles with negligible performance degradation.

As schematically shown in Figure 1, our design takes advantage of the high surface area (~100 m^2/g)[11] and good conductivity ($\rho \approx 10\ \mu\Omega\cdot$cm)[12] offered by the $TiSi_2$ nanonet.[13] Important to our design, the $TiSi_2$ nanonet exhibits no significant reactivity toward oxygen reduction or evolution when examined in the dimethoxyethane (DME) or tetraethylene glycol dimethyl ether (TEGDME) electrolyte systems (Figures S2 and S3 in Supporting Information, SI). By comparison, many forms of carbon have proven catalytically active toward oxygen reduction reaction (ORR).[14] While the ORR reactivity may be perceived as an advantage because it helps reduce discharge overpotentials, the reactivity also creates a critical problem. For instance, on the one hand, carbon is susceptible to reactions with the superoxide anion (O_2^-) that is an important intermediate during discharge,[15] leading to cathode erosion over repeated charge/discharge.[16] On the other hand, ORR activity by carbon produces Li_2O_2 products at

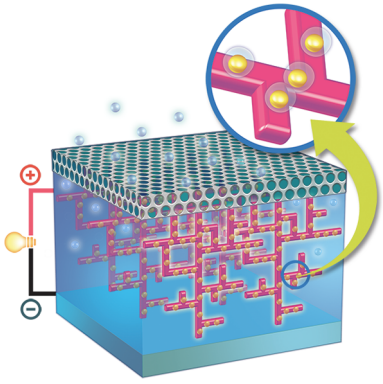

Figure 1. Schematic illustration of the overall design. Two-dimensional $TiSi_2$ nanonets are grown on a metal foam to be used directly as an air cathode without binders or other additives. Ru nanoparticles (golden balls in the magnified view) preferably deposit on the b planes of $TiSi_2$. Li_2O_2 particles (semitransparent spheres surrounding golden balls) form and decompose around Ru catalysts.

Received: May 7, 2014
Published: June 11, 2014

   dx.doi.org/10.1021/ja504431k | J. Am. Chem. Soc. 2014, 136, 8903−8906

locations away from oxygen evolution reaction (OER) catalysts, artificially increasing overpotentials necessary to decompose Li_2O_2 during recharge. This is because carbon only catalyzes ORR but not OER. As a result, high recharge potentials, especially toward the end of the recharge cycle, are required to fully decompose Li_2O_2. The electrolyte and carbon support are known to decompose at such high potentials.[5,17] These negative influences can be mitigated by the application of a noncarbon cathode support that does not catalyze ORR. The $TiSi_2$ nanonet meets the need.

To promote ORR, we chose to modify the surface of $TiSi_2$ with Ru nanoparticles. Less active than Pt and Pd but more so than Au in terms of ORR activities,[14] Ru costs much less than the other precious metals. Nanoparticles of Ru have been shown to be active toward ORR in nonaqueous systems as well.[9,18,19] More important, unlike Pt, Ru does not promote electrolyte decomposition.[20] For this proof-of-concept demonstration, Ru was grown on $TiSi_2$ by atomic layer deposition (ALD) to afford ligand-free surfaces for better catalytic activities. Intriguingly, site-selective growth was obtained, and Ru nanoparticles were observed only on the top and bottom surfaces of C49 $TiSi_2$ (Figure 2c and 2d), similar to our previous observations of Pt nanoparticle growth on the $TiSi_2$ nanonet.[21] To understand what governs the unique site selectivity, we carried out density functional theory (DFT) calculations, where the metal was modeled as a 38-atom cluster and $TiSi_2$ was treated as a 6-layer slab (see Experimental Section in SI). After optimization, a strong mixing at the interface between Ru_{38} and C49 $TiSi_2$ is obvious (Figure 2a), suggesting greater interaction between the Ru nanoparticle and the Si layer of the b planes in $TiSi_2$. The degree of such interfacial interaction is much weaker in the a or c plane as evidenced in Figure 2b. The difference is quantified by the adsorption energy of the nanoparticle on the two $TiSi_2$ surfaces: −54 eV on the b-plane and −38 eV on the c-plane. The preferred adsorption of Ru onto the b-plane can also be viewed from the adhesion perspective. Using the area of the interface (ca. 110 Å), an adhesion energy of −7.8 J/m^2 is obtained for the Ru/$TiSi_2$-*b*-plane interface. This value is much higher than the typical metal/silicide adhesion (e.g., −3.85 J/m^2 between Fe and $MoSi_2$).[22] Similar DFT results were obtained for the Pt/$TiSi_2$ system (Figure S11).[21] It is noted that the growth of Ru was not yet optimized in terms of size distribution (Figure 2c inset) because this proof-of-concept work is intended to examine the suitability of the $TiSi_2$ nanonet as a support for Li–O_2 battery operations. Should it become necessary to achieve uniform size distribution, the system can be readily optimized by adjusting the ALD growth parameters, as has been shown in the case of bimetallic nanoparticles preparation reported by J. Elam et al.[23] It is also noted that the alloying between Ru and Si as shown in Figure 2 is not expected to significantly alter the electrochemical properties of the Ru catalyst as discussed next.

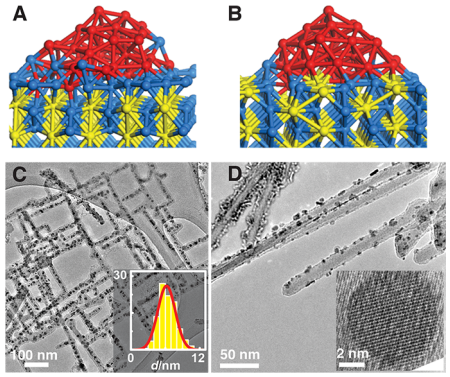

Figure 2. Site-selective growth of Ru nanoparticles on $TiSi_2$ nanonets. DFT calculations show that Ru clusters prefer the b planes (A) over the c planes of C49 $TiSi_2$ (B). The prediction is consistent with experimental observations by TEM from the top (C), where b planes are parallel to the viewing direction. Inset: size distribution of Ru nanoparticles by a 100-cycle ALD growth. When viewed from the side (D), where b planes are perpendicular to the viewing direction, no Ru nanoparticles are seen on the c or a planes. Inset: high-resolution TEM confirming the crystalline nature of the Ru nanoparticles.

The activity of the Ru/$TiSi_2$ system was next characterized in the DME electrolyte. For the first cycle upon discharge, a plateau at 2.65 V was obtained, corresponding to a kinetic overpotential of 0.31 V at 200 mA/g_{Ru} (all capacities normalized to the mass loading of Ru; see SI for more details). When the polarity of current was switched, the recharge potential was first on a fast rising slope, reaching 3.39 V at 20% of the full discharged capacity. The potential increase slowed afterward, reaching a pseudo plateau with an average potential of 3.64 V between 20% and 100% of the full discharge capacity. At the end of the recharge cycle, a potential of 3.86 V was measured. Remarkably, the discharge plateau potential for the 100th cycle was only 45 mV more negative than that of the first cycle. The recharge plateau potential increased by 111 mV for the 100th cycle when compared with the first one. To quantify the round-trip efficiencies, the average recharge potential was divided by the average discharge one, and the data were plotted in Figure 3b. The round-trip efficiency was consistently >70%, representing one of the highest in the literature.

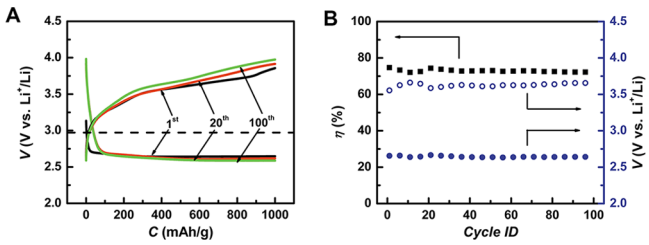

Figure 3. Electrochemical characterization of the Ru/$TiSi_2$ cathode in DME (0.1 M $LiClO_4$). (A) Potential vs capacity plots of a cell during the 1st, 20th, and 100th cycle, respectively. The capacity was normalized to the mass of Ru catalysts. The dotted horizontal line marks the thermodynamic equilibrium potential of 2.96 V. (B) Average discharge (solid circle), recharge (hollow circle), and round-trip efficiencies over 100 cycles. For clarity, one data point for every 5 cycles is shown (see Figure S12 for complete plots).

It has been previously shown that the decomposition of the electrode or the electrolyte or both could yield discharge/charge characteristics similar to what is presented above. It is therefore of critical importance to confirm that the recorded performance was indeed a measure of the reversible conversion between O_2 and Li_2O_2. For this purpose, we next employed differential electrochemical mass spectrometry (DEMS), Raman spectroscopy, transmission electron microscopy (TEM), and X-ray photoelectron spectroscopy (XPS) to examine the products.

DEMS was set up to detect the recharge products. For a true reversible conversion of Li_2O_2, every 2 e^-'s passed would

dx.doi.org/10.1021/ja504431k | J. Am. Chem. Soc. 2014, 136, 8903–8906

produce 1 gaseous O_2 molecule.[24] Other than O_2, CO_2 is a common byproduct due to decomposition of carbonate, whose appearance would indicate undesired side reactions such as electrode or electrolyte decomposition that produce inorganic and organic carbonates. As is shown in Figure 4a, two O_2-

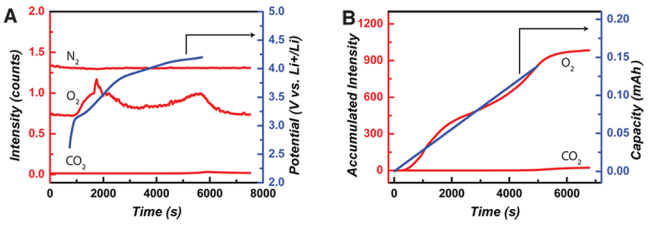

Figure 4. Detection of recharge products. (A) Real time mass spectrometry detection of gases generated at a fast 500 mA/g_{Ru} charging rate. (B) Accumulated counts of CO_2 and O_2. Data collected in 1.0 M $LiClO_4$ in TEGDME.

production peaks were observed during recharge, one at ca. 20% of the full discharge capacity and the other at a very late stage of recharge. Although the in situ O_2-detection shown in Figure 4a does not take into account the complex mass transport within the test cell and, as such, may not reflect the true instantaneous O_2 release characteristics, the two-stage decomposition of Li_2O_2 is qualitatively accurate. The characteristics are consistent with the mechanistic switch of the Li_2O_2 decomposition at different stages of recharge proposed by Shao-Horn et al.[25] The results that O_2 evolution happens at two voltages are also consistent with what has been reported by Bruce et al.[10] Important to our discussion, minimum CO_2 (the product of carbonate decomposition) was detected, supporting that carbonates formed during discharge/recharge were insignificant. The conclusion was later confirmed by Raman spectroscopy. It is noted that electrolyte (DME or TEGDME) instability is a known issue,[26] the decomposition of which produces carbonates. Because the cathode studied here is carbon free, any observed carbonate is likely a result of electrolyte decomposition.

To ensure the measured O_2 was not a result of cell leakage from ambient air, N_2 was constantly monitored as an internal reference, which remained constant during the experiment (Figure 4a), supporting the measured O_2 reflects Li_2O_2 decomposition. The total charge was obtained by integrating the calibrated intensity over time, and the result was plotted in Figure 4b. It is noted that the DEMS results were collected at a significantly higher charge rate (500 mA/g_{Ru}) than the rate under which cyclability data were presented (200 mA/g_{Ru}). A fast rate was necessary to meet the real-time detection limit of the mass spectrometer used for this study. The actual cell used to measure the cyclability was studied at a much slower discharge/charge rate. Using a separate injection method, we obtained a faradaic efficiency of 94.1% (see Experimental Section in SI). The result is quantitatively consistent with literature reports of O_2 detection by similar methods.[24] The detection establishes that the observed charge/discharge behavior was indeed a measure of Li_2O_2 formation and decomposition. By comparison, Ru/CB showed a poor rate capability. The test cell could only recover a small portion of discharged capacity during a fast recharge when the upper cut off voltage was limited to 4.2 V (used for Ru/$TiSi_2$ as shown in Figure 4a). When the upper cutoff voltage was increased to 4.5 V, significant CO_2 generation was detected (see SI). The comparison highlights the stability of the Ru/$TiSi_2$ system over Ru/C.

The formation of Li_2O_2 was directly observed by TEM (Figure 5a). Due to the known instability of Li_2O_2 under

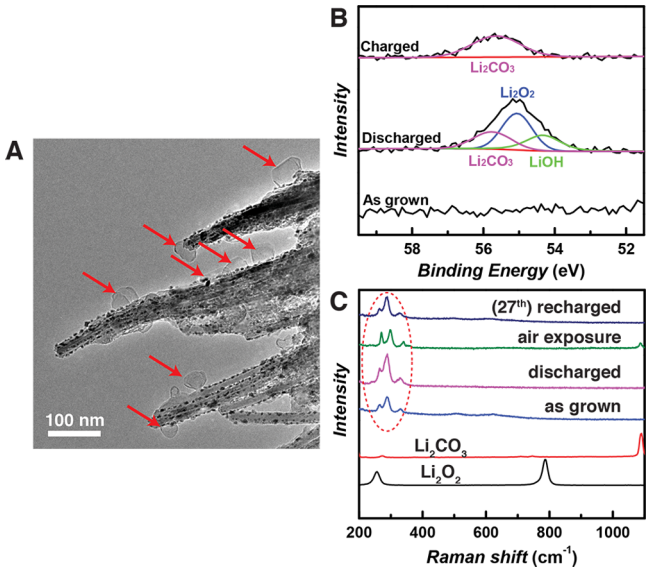

Figure 5. Product detection. (A) TEM showing the morphology of Li_2O_2 (highlighted by arrows). (B) Li 1s peaks of Ru/$TiSi_2$ cathode at different stages by XPS. (C) Raman spectra of Ru/$TiSi_2$ cathode at different stages. Reference spectra of Li_2O_2 and Li_2CO_3 of commercial samples are shown at the bottom. The peaks between 200 and 400 cm^{-1} (outlined by a dotted circle) are indicative of C49 $TiSi_2$.

focused electron beams,[27] we were unable to study the crystallinity of the product. Nevertheless, particles of 20−30 nm in diameters were abundant (Figure 5a). The existence of Li_2O_2 was also confirmed by XPS. Upon recharge, the deconvoluted peak that can be assigned to Li_2O_2[28,29] disappeared (Figure 5b). Because our XPS experiment involved a brief exposure of the samples to ambient air (see SI for experimental procedures), Li_2CO_3 was likely formed by reactions between Li_2O_2 and CO_2 during the exposure. Correspondingly, a Li_2CO_3 peak was persistent at all stages of the XPS characterizations (discharged and recharged, Figure 5b). As noted previously, the employment of a noncarbon cathode does not address instability issues of the electrolyte. Carbonate formation due to DME or TEMDME decomposition cannot be ruled out. It is another important reason why carbonates were observed in the XPS spectra.

Lastly, we used Raman spectroscopy to identify the chemical nature of as-prepared, discharged, and recharged Ru/$TiSi_2$ samples, respectively. Our goal was to observe whether Li_2CO_3 formed during the reactions. As shown in Figure 5c, other than the sample exposed to ambient air, no Li_2CO_3 was seen, suggesting that no significant Li_2CO_3 formation or accumulation took place. We caution that the absence of Raman signals alone is inadequate to rule out the formation of Li_2CO_3. The conclusion is supported by our DEMS data presented earlier in this communication. The lack of Li_2CO_3 on the Ru/$TiSi_2$ sample is understood as a result of improved stability by the usage of a noncarbon cathode support. Our attempt to directly observe the Raman signal corresponding to Li_2O_2 fell short. It is possible that the discharge products are of poor crystallinity under our test conditions (rate: 200 mA/g_{Ru}).

dx.doi.org/10.1021/ja504431k | J. Am. Chem. Soc. 2014, 136, 8903−8906

It is also possible that the electrochemically grown Li_2O_2 is fundamentally different from the commercial Li_2O_2 reference used to generate Figure 5c.[30] It is noted that the lack of Li_2O_2 Raman peaks has been reported by other researchers as well and is not unique to our system.[31] The existence of Li_2O_2 may be indirectly confirmed by exposing the discharged sample to ambient air, which would produce Li_2CO_3 upon reaction with CO_2 and H_2O. This was indeed observed in our experiments (green trace in Figure 5c). Taken as a whole, the DEMS, TEM, XPS, and Raman characterizations collectively support that the electrochemical characteristics presented in Figure 3 are a reflection of reversible formation and decomposition of Li_2O_2. The extensive cyclability (>100 cycles) is among the best reported on any cathode materials in the literature.

Reversible formation and decomposition of Li_2O_2 is key to the successful operation of a rechargeable aprotic Li−O_2 cell. As an important step toward this goal, we presented a Ru-nanoparticles-decorated $TiSi_2$ nanonet as a new cathode system. Compared with the popularly used carbon support, the $TiSi_2$ nanonet is advantageous in that it does not show measurable reactivity toward reaction intermediates such as superoxide ions. As a result, extensive cyclability (>100 cycles) with confirmed Li_2O_2 formation and decomposition was obtained. The new cathode system is expected to play positive roles in the fundamental understanding of electrolyte stability as well because of its inert nature.

■ ASSOCIATED CONTENT

Supporting Information

Experimental details and additional results. This material is available free of charge via the Internet at http://pubs.acs.org

■ AUTHOR INFORMATION

Corresponding Author

dunwei.wang@bc.edu

Author Contributions

[§]J.X. and X.Y. contributed equally.

Notes

The authors declare no competing financial interest.

■ ACKNOWLEDGMENTS

The work is supported by Boston College. D.W. is an Alfred P. Sloan Fellow. We thank G. McMahon, J. Morabito, H. Wu, and G. Chen for their technical assistance. We also thank Y. Shao-Horn and her group for insightful discussions. XPS was performed at the Center for Nanoscale Systems (CNS).

■ REFERENCES

(1) Choi, N.-S.; Chen, Z.; Freunberger, S. A.; Ji, X.; Sun, Y.-K.; Amine, K.; Yushin, G.; Nazar, L. F.; Cho, J.; Bruce, P. G. *Angew. Chem., Int. Ed.* **2012**, *51*, 9994.

(2) Girishkumar, G.; McCloskey, B.; Luntz, A. C.; Swanson, S.; Wilcke, W. *J. Phys. Chem. Lett.* **2010**, *1*, 2193.

(3) Bruce, P. G.; Freunberger, S. A.; Hardwick, L. J.; Tarascon, J. M. *Nat. Mater.* **2012**, *11*, 19.

(4) Lu, Y. C.; Gallant, B. M.; Kwabi, D. G.; Harding, J. R.; Mitchell, R. R.; Whittingham, M. S.; Shao-Horn, Y. *Energy Environ. Sci.* **2013**, *6*, 750.

(5) Thotiyl, M. M. O.; Freunberger, S. A.; Peng, Z. Q.; Bruce, P. G. *J. Am. Chem. Soc.* **2013**, *135*, 494.

(6) Lu, J.; Lei, Y.; Lau, K. C.; Luo, X. Y.; Du, P.; Wen, J. G.; Assary, R. S.; Das, U.; Miller, D. J.; Elam, J. W.; Albishri, H. M.; Abd El-Hady, D.; Sun, Y. K.; Curtiss, L. A.; Amine, K. *Nat. Commun.* **2013**, *4*, 2383.

(7) McCloskey, B. D.; Speidel, A.; Scheffler, R.; Miller, D. C.; Viswanathan, V.; Hummelshøj, J. S.; Nørskov, J. K.; Luntz, A. C. *J. Phys. Chem. Lett.* **2012**, *3*, 997.

(8) Peng, Z.; Freunberger, S. A.; Chen, Y.; Bruce, P. G. *Science* **2012**, *337*, 563.

(9) Li, F.; Tang, D.-M.; Chen, Y.; Golberg, D.; Kitaura, H.; Zhang, T.; Yamada, A.; Zhou, H. *Nano Lett.* **2013**, *13*, 4702.

(10) Ottakam Thotiyl, M. M.; Freunberger, S. A.; Peng, Z.; Chen, Y.; Liu, Z.; Bruce, P. G. *Nat. Mater.* **2013**, *12*, 1050.

(11) Lin, Y.; Zhou, S.; Liu, X.; Sheehan, S.; Wang, D. *J. Am. Chem. Soc.* **2009**, *131*, 2772.

(12) Zhou, S.; Liu, X.; Lin, Y.; Wang, D. *Angew. Chem., Int. Ed.* **2008**, *47*, 7681.

(13) Zhou, S.; Yang, X.; Xie, J.; Simpson, Z. I.; Wang, D. *Chem. Commun.* **2013**, *49*, 6470.

(14) Lu, Y. C.; Gasteiger, H. A.; Shao-Horn, Y. *J. Am. Chem. Soc.* **2011**, *133*, 19048.

(15) Yang, J.; Zhai, D.; Wang, H.-H.; Lau, K. C.; Schlueter, J. A.; Du, P.; Myers, D. J.; Sun, Y.-K.; Curtiss, L. A.; Amine, K. *Phys. Chem. Chem. Phys.* **2013**, *15*, 3764.

(16) Gallant, B. M.; Mitchell, R. R.; Kwabi, D. G.; Zhou, J.; Zuin, L.; Thompson, C. V.; Shao-Horn, Y. *J. Phys. Chem. C* **2012**, *116*, 20800.

(17) McCloskey, B. D.; Valery, A.; Luntz, A. C.; Gowda, S. R.; Wallraff, G. M.; Garcia, J. M.; Mori, T.; Krupp, L. E. *J. Phys. Chem. Lett.* **2013**, *4*, 2989.

(18) Jung, H.-G.; Jeong, Y. S.; Park, J.-B.; Sun, Y.-K.; Scrosati, B.; Lee, Y. J. *ACS Nano* **2013**, *7*, 3532.

(19) Li, F.; Chen, Y.; Tang, D.-M.; Jian, Z.; Liu, C.; Golberg, D.; Yamada, A.; Zhou, H. *Energy Environ. Sci.* **2014**, *7*, 1648.

(20) Harding, J. R.; Lu, Y. C.; Tsukada, Y.; Shao-Horn, Y. *Phys. Chem. Chem. Phys.* **2012**, *14*, 10540.

(21) Xie, J.; Yang, X. G.; Han, B. H.; Shao-Horn, Y.; Wang, D. W. *ACS Nano* **2013**, *7*, 6337.

(22) Jiang, D. E.; Carter, E. A. *Acta Mater.* **2005**, *53*, 4489.

(23) Lu, J.; Low, K.-B.; Lei, Y.; Libera, J. A.; Nicholls, A.; Stair, P. C.; Elam, J. W. *Nat. Commun.* **2014**, *5*, 3264.

(24) McCloskey, B. D.; Bethune, D. S.; Shelby, R. M.; Girishkumar, G.; Luntz, A. C. *J. Phys. Chem. Lett.* **2011**, *2*, 1161.

(25) Gallant, B. M.; Kwabi, D. G.; Mitchell, R. R.; Zhou, J. G.; Thompson, C. V.; Shao-Horn, Y. *Energy Environ. Sci.* **2013**, *6*, 2518.

(26) Freunberger, S. A.; Chen, Y.; Drewett, N. E.; Hardwick, L. J.; Bardé, F.; Bruce, P. G. *Angew. Chem., Int. Ed.* **2011**, *50*, 8609.

(27) Zhong, L.; Mitchell, R. R.; Liu, Y.; Gallant, B. M.; Thompson, C. V.; Huang, J. Y.; Mao, S. X.; Shao-Horn, Y. *Nano Lett.* **2013**, *13*, 2209.

(28) Lei, Y.; Lu, J.; Luo, X. Y.; Wu, T. P.; Du, P.; Zhang, X. Y.; Ren, Y.; Wen, J. G.; Miller, D. J.; Miller, J. T.; Sun, Y. K.; Elam, J. W.; Amine, K. *Nano Lett.* **2013**, *13*, 4182.

(29) Younesi, R.; Hahlin, M.; Björefors, F.; Johansson, P.; Edström, K. *Chem. Mater.* **2012**, *25*, 77.

(30) Yilmaz, E.; Yogi, C.; Yamanaka, K.; Ohta, T.; Byon, H. R. *Nano Lett.* **2013**, *13*, 4679.

(31) Zhai, D.; Wang, H.-H.; Yang, J.; Lau, K. C.; Li, K.; Amine, K.; Curtiss, L. A. *J. Am. Chem. Soc.* **2013**, *135*, 15364.